Glucose-linked sub-50-nm unimer polyion complex-assembled gold nanoparticles for targeted siRNA delivery to glucose transporter 1-overexpressing breast cancer stem-like cells

Yu Yi, Hyun Jin Kim, Meng Zheng, Peng Mi, Mitsuru Naito, Beob Soo Kim, Hyun Su Min, Kotaro Hayashi, Federico Perche, Kazuko Toh, et al.

▶ **To cite this version:**

Yu Yi, Hyun Jin Kim, Meng Zheng, Peng Mi, Mitsuru Naito, et al.. Glucose-linked sub-50-nm unimer polyion complex-assembled gold nanoparticles for targeted siRNA delivery to glucose transporter 1-overexpressing breast cancer stem-like cells. Journal of Controlled Release, 2019, 295, pp.268 - 277. 10.1016/j.jconrel.2019.01.006 . hal-02995629

HAL Id: hal-02995629
https://hal.science/hal-02995629v1

Submitted on 9 Nov 2020

HAL is a multi-disciplinary open access archive for the deposit and dissemination of scientific research documents, whether they are published or not. The documents may come from teaching and research institutions in France or abroad, or from public or private research centers.

L'archive ouverte pluridisciplinaire **HAL**, est destinée au dépôt et à la diffusion de documents scientifiques de niveau recherche, publiés ou non, émanant des établissements d'enseignement et de recherche français ou étrangers, des laboratoires publics ou privés.

Accepted Manuscript

Glucose-linked sub-50-nm unimer polyion complex-assembled gold nanoparticles for targeted siRNA delivery to glucose transporter 1-overexpressing breast cancer stem-like cells

Yu Yi, Hyun Jin Kim, Meng Zheng, Peng Mi, Mitsuru Naito, Beob Soo Kim, Hyun Su Min, Kotaro Hayashi, Federico Perche, Kazuko Toh, Xueying Liu, Yuki Mochida, Hiroaki Kinoh, Horacio Cabral, Kanjiro Miyata, Kazunori Kataoka

PII: S0168-3659(19)30022-7
DOI: https://doi.org/10.1016/j.jconrel.2019.01.006
Reference: COREL 9606

To appear in: *Journal of Controlled Release*

Received date: 30 July 2018
Revised date: 18 December 2018
Accepted date: 7 January 2019

Please cite this article as: Yu Yi, Hyun Jin Kim, Meng Zheng, Peng Mi, Mitsuru Naito, Beob Soo Kim, Hyun Su Min, Kotaro Hayashi, Federico Perche, Kazuko Toh, Xueying Liu, Yuki Mochida, Hiroaki Kinoh, Horacio Cabral, Kanjiro Miyata, Kazunori Kataoka , Glucose-linked sub-50-nm unimer polyion complex-assembled gold nanoparticles for targeted siRNA delivery to glucose transporter 1-overexpressing breast cancer stem-like cells. Corel (2019), https://doi.org/10.1016/j.jconrel.2019.01.006

This is a PDF file of an unedited manuscript that has been accepted for publication. As a service to our customers we are providing this early version of the manuscript. The manuscript will undergo copyediting, typesetting, and review of the resulting proof before it is published in its final form. Please note that during the production process errors may be discovered which could affect the content, and all legal disclaimers that apply to the journal pertain.

ACCEPTED MANUSCRIPT

Glucose-linked sub-50-nm unimer polyion complex-assembled gold nanoparticles for targeted siRNA delivery to glucose transporter 1-overexpressing breast cancer stem-like cells

Yu Yi[1,2], Hyun Jin Kim[3], Meng Zheng[1,4], Peng Mi[5,6], Mitsuru Naito[3], Beob Soo Kim[1], Hyun Su Min[1], Kotaro Hayashi[5], Federico Perche[3,7], Kazuko Toh[5], Xueying Liu[5], Yuki Mochida[5], Hiroaki Kinoh[5], Horacio Cabral[8], Kanjiro Miyata[1,3,*] and Kazunori Kataoka[5,9,*]

[1]*Department of Materials Engineering, Graduate School of Engineering, The University of Tokyo, 7-3-1 Hongo, Bunkyo-ku, Tokyo 113-8656, Japan*
[2]*CAS Center for Excellence in Nanoscience, CAS Key Laboratory for Biological Effects of Nanomaterials and Nanosafety, National Center for Nanoscience and Technology (NCNST), No. 11 Beiyitiao, Zhongguancun, Beijing 100190, China*
[3]*Center for Disease Biology and Integrative Medicine, Graduate School of Medicine, The University of Tokyo, 7-3-1 Hongo, Bunkyo-ku, Tokyo 113-0033, Japan*
[4]*International Joint Center for Biomedical Innovation, School of Life Sciences, Henan University, Kaifeng, Henan, 475004, China*
[5]*Innovation Center of Nanomedicine, Kawasaki Institute of Industrial Promotion, 3-25-14 Tonomachi, Kawasaki-ku, Kawasaki 210-0821, Japan*
[6]*Department of Radiology, Center for Medical Imaging, and State Key Laboratory of Biotherapy, West China Hospital, Sichuan University, Collaborative Innovation Center for Biotherapy, Chengdu, Sichuan 610041, China*
[7]*Centre de Biophysique Moléculaire, CNRS UPR 4301, Rue Charles Sadron – CS 80054, 45071 Orléans Cedex 2, France*
[8]*Department of Bioengineering, Graduate School of Engineering, The University of Tokyo, 7-3-1 Hongo, Bunkyo-ku, Tokyo 113-8656, Japan*
[9]*Policy Alternatives Research Institute, The University of Tokyo, 7-3-1 Hongo, Bunkyo-ku, Tokyo 113-0033, Japan*

***Corresponding authors:**
Kazunori Kataoka, Ph.D.
Director General,
Innovation Center of Nanomedicine, Kawasaki Institute of Industrial Promotion, 3-25-14 Tonomachi, Kawasaki-ku, Kawasaki 210-0821, Japan.
Phone: +81-44-589-5812
FAX: +81-44-589-5832
E-mail: kataoka@pari.u-tokyo.ac.jp

Kanjiro Miyata, Ph.D.
Associate Professor,
Department of Materials Engineering, Graduate School of Engineering, The University of Tokyo, 7-3-1 Hongo, Bunkyo-ku, Tokyo 113-8656, Japan.

ACCEPTED MANUSCRIPT

Phone: +81-3-5841-0862
FAX: +81-3-5841-7139
E-mail: miyata@bmw.t.u-tokyo.ac.jp

ABSTRACT

Cancer stem-like cells (CSCs) treatment is a plausible strategy for enhanced cancer therapy. Here we report a glucose-installed sub-50-nm nanocarrier for the targeted delivery of small interfering RNA (siRNA) to CSCs through selective recognition of the glucose ligand to the glucose transporter 1 (GLUT1) overexpressed on the CSC surface. The siRNA nanocarrier was constructed via a two-step assembling process. First, a glucose-installed poly(ethylene glycol)-*block*-poly(L-lysine) modified with lipoic acid (LA) at the ω-end (Glu-PEG-PLL-LA) was associated with a single siRNA to form a unimer polyion complex (uPIC). Second, a 20 nm gold nanoparticle (AuNP) was decorated with ~65 uPICs through Au-S bonding. The glucose-installed targeted nanoparticles (Glu-NPs) exhibited higher cellular uptake of siRNA payloads in a spheroid breast cancer (MBA-MB-231) cell culture compared with glucose-unconjugated control nanoparticles (MeO-NPs). Notably, the Glu-NPs became more efficiently internalized into the CSC fraction, which was defined by aldehyde dehydrogenase (ALDH) activity assay, than the other fractions, probably due to the higher GLUT1 expression level on the CSCs. The Glu-NPs elicited significantly enhanced gene silencing in a CSC-rich orthotopic MDA-MB-231 tumor tissue following systemic administration to tumor-bearing mice. Ultimately, the repeated administrations of polo-like kinase 1 (PLK1) siRNA-loaded Glu-NPs significantly suppressed the growth of orthotopic MDA-MB-231 tumors. These results demonstrate that Glu-NP is a promising nanocarrier design for CSC-targeted cancer treatment.

Keywords: Glucose, Cancer stem-like cell, siRNA delivery, Polyion complex, Gold nanoparticle

1. Introduction

Breast cancer is one of the most common cancers in women [1]. Breast cancer patients are at a high risk of tumor recurrence and metastasis despite a high survival rate after treatments. Recent studies have shown that cancer stem-like cells (CSCs) are highly involved in drug resistance, metastasis, and the relapse of breast cancers due to their self-renewal ability and multilineage differentiation capacity [2]. CSC-targeted treatment is, therefore, a promising strategy for improving the efficacy of breast cancer therapy [3, 4]. Different approaches have been reported for the selective treatment of CSCs, by either inhibiting the CSC signal pathways [5], suppressing the protein kinases in CSCs [6, 7], modulating the CSC-niches [8], reprogramming the metabolism of CSCs [9], or differentiating the CSCs [10]. The targeting of CSC biomarkers, such as CD44, has attracted much attention in CSC-specific drug delivery [11]. Biomacromolecules, such as antibodies, aptamers, and peptides, have been equipped on the surface of nanomedicines as a CSC-targeting ligand [12-14], yet there still be issues on cost, stability, and efficacy [15, 16]. Efficient, facile, and stable ligands are, therefore, highly desirable for active CSC targeting. It has long been recognized that glucose transporter (GLUT) is overexpressed on various types of cancer cells due to the Warburg effect, an insufficient

ACCEPTED MANUSCRIPT

glycolysis pathway to generate adenosine triphosphate (ATP) [17]. Recent studies have shown that glucose metabolism is even more active in CSCs [18], suggesting that the GLUT is a promising candidate for CSC-targeted treatments using a glucose-installed nanomedicine [19, 20].

RNA interference (RNAi) technology has attracted great interest for cancer therapy, where small interfering RNA (siRNA) is used in sequence-specific silencing of the messenger RNA (mRNA) coding cancer-related proteins in mammalian cells [21-23]. While CSCs are inert to traditional chemotherapeutics due to numerous resistance mechanisms, such as multidrug efflux transporters, they are sensitive to drugs that impair particular survival signals, and can, therefore, be selectively targeted by siRNA [24]. This indicates the great potential of RNAi technology in CSC therapy. Tremendous efforts have been made to develop nanocarriers for systemic delivery of siRNA, which has solved the problem of the poor bioavailability of naked siRNA due to RNases degradation, rapid renal clearance in the bloodstream, and inferior cellular internalization. These nanocarriers have been constructed from lipids, polymers [25-28], and/or inorganic nanoparticles [29-32]. Several lipid- and polymer-based delivery vehicles have been enrolled in clinical trials to date [33]. These nano-sized vehicles are able to extravasate through the leaky tumor vasculature to accumulate in solid tumors [34], with a recent study emphasizing the advantages of sub-50-nm nanoparticles for efficient permeation in thick fibrotic tumor models [35, 36]. Furthermore, tumor-targeting ligands have also been installed on the surface of siRNA-loaded nanocarriers for more efficient binding to the target cells based on ligand-receptor interactions, which improves the delivery efficacy to tumors with reduced side effects to normal tissue [37, 38].

Here we present the development of a glucose-installed sub-50-nm unimer polyion complex-assembled gold nanoparticle (Glu-NP) for systemic delivery of siRNA to a CSC-rich breast cancer model. This Glu-NP is constructed via a two-step bottom-up self-assembly of unimer polyion complexes (uPICs) and a gold nanoparticle (AuNP) (Fig. 1). The Glu-NP as well as MeO-NP should release siRNA payloads in the glutathione-rich environment in the cell via the exchange reaction in Au-S bonds [39]. Our previous research has demonstrated the advantages of uPIC-AuNPs, including size tunability, a prolonged blood circulation property, and ligand-mediated targetability, all of which lead to enhanced siRNA accumulation in subcutaneous tumor models [39, 40]. Here we installed the glucose to the α-end of poly(ethylene glycol) (PEG)-*block*-poly(L-lysine) by an ether linkage at the C6 position. Particularly, the C6 modification of glucose largely remains its recognition ability to GLUT1 [41], endowing the Glu-NPs with a specific targeting capability toward GLUT1. We demonstrate that the Glu-NPs more specifically recognize CSCs in MDA-MB-231 breast cancer spheroid cultures and enhance antitumor efficacy in an orthotopic breast tumor model, therefore highlighting the potential of Glu-installed nanomedicines for successful breast cancer therapy.

ACCEPTED MANUSCRIPT

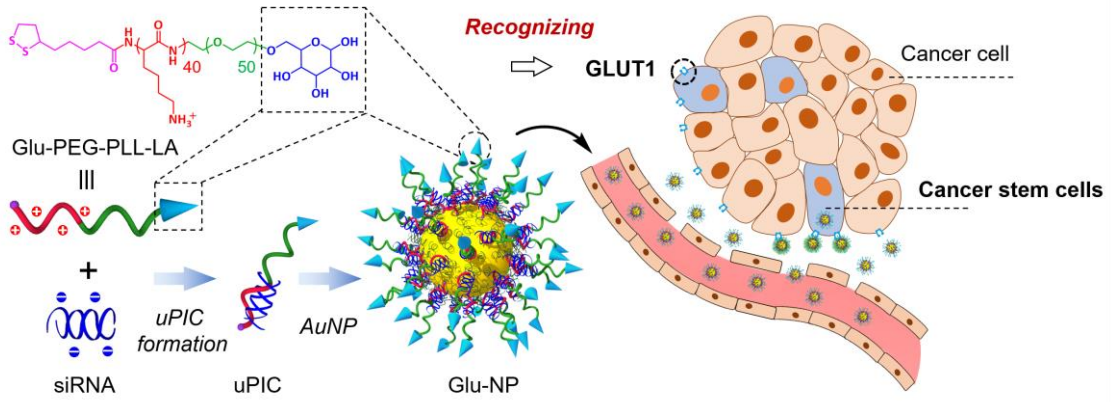

Fig. 1. Schematic illustration of Glu-NP preparation from Glu-PEG-PLL-LA, siRNA, and AuNP. The Glu-NP was engineered via a two-step self-assembling approach. First, the uPIC was formed between a single pair of siRNA and Glu-installed PEG-block-catiomer through charge-matched neutralization. Second, the monodispersed Glu-NP was obtained from the decoration of a 20 nm AuNP with uPICs through Au-S coordination. The PEG protection and sub-50-nm size contribute to a prolonged blood circulation property and efficient tumor accumulation. The Glu ligand endows the Glu-NPs with targetability toward breast CSCs by binding to GLUT1.

2. Materials and methods

2.1. Materials

α-Methoxy-ω-amino poly(ethylene glycol) (MeO-PEG-NH_2; molecular weight (MW): 2200) was purchased from NOF Co., Inc. (Tokyo, Japan). α-1,2-*O*-Isopropylidene-3,5-*O*-benzylidene-*D*-glucofuranose-ω-amino PEG (BIG-PEG-NH_2; MW: 2200) was synthesized as described previously [42]. *N*-Carboxy anhydride of ε-trifluoroacetyl-L-lysine (Lys(TFA)-NCA) was bought from Chuo Kaseihin Co., Inc. (Tokyo, Japan). *N*-Hydroxysuccinimidyl ester of lipoic acid (LA-NHS) was synthesized according to the previous report [43]. *N*,*N*-Dimethylformamide (DMF), dimethyl sulfoxide (DMSO, >99%), trisodium citrate dihydrate ($Na_3Ct{\cdot}2H_2O$, >99%), *N*,*N*-diisopropylethylamine (DIPEA), chemically synthesized phloretin, and RPMI 1640 medium were purchased from Wako Pure Chemical Industries, Ltd. (Tokyo, Japan). Gold(III) chloride trihydrate ($HAuCl_4{\cdot}3H_2O$, 99.9%), D_2O (99.9%), tetramethylsilane (TMS, 99.5%), poly(ethylene glycol) methyl ether thiol (PEG-SH; MW: 800), ethylenediaminetetraacetic acid (EDTA), 5,5′-dithiobis(2-nitrobenzoic acid) (Ellman's reagent), and serum-free DMEM-F12 medium were purchased from Sigma Aldrich (St. Louis, MO, USA). The ultrapure DNase/RNase-free distilled water (Thermo Fisher Scientific Inc., Waltham, MA, USA), cell counting kit 8 (CCK-8, Dojindo Laboratories, Kumamoto, Japan), sterile 4-(2-hydroxyethyl)-1-piperazineethanesulfonic acid (HEPES) buffer (Amresco, Solon, OH, USA), and fetal bovine serum (FBS) (Dainippon Sumitomo Pharma Co., Ltd., Osaka, Japan) were used as received. Citrate-capped AuNPs with a hydrodynamic diameter of 20 nm were prepared according to the Turkevich method through reduction of chloroauric acid ($HAuCl_4$) with sodium citrate (Na_3Ct) [44]. All siRNAs used in this work were

ACCEPTED MANUSCRIPT

synthesized by Hokkaido System Science (Hokkaido, Japan) or Gene Design (Osaka, Japan). Their sequences were as follows: (1) polo-like kinase 1 (PLK1) siRNA (siPLK1): 5′-AGA uCA CCC uCC UuA AAu AUU-3′ (sense), 5′-UAU UUA AgG AGG GUG AuC UUU-3′ (antisense), where uppercase and lowercase letters represent RNA and 2′-*O*-methylated RNA, respectively; (2) control siRNA (siCont): 5′-UUC UCC GAA CGU GUC ACG UdTdT-3′ (sense), 5′-ACG UGA CAC GUU CGG AGA AdTdT-3′ (antisense); (3) Alexa647 dye-labeled siRNA (Alexa647-siRNA): 5′-CUU ACG CUG AGU ACU UCG AdTdT-3′ (sense) with Alexa647 dye on the 5′-end, 5′-UCG AAG UAC UCA GCG UAA GdTdT-3′ (antisense). NOD/SCID mice and BALB/c nude mice (female; 6 weeks old) were purchased from Charles River Japan (Kanagawa, Japan). All the animal experiments were conducted under the Guidelines for the Care and Use of Laboratory Animals of The University of Tokyo.

2.2. Synthesis of glucose-poly(ethylene glycol)-b-poly(L-lysine) modified with lipoic acid at the ω-terminal (Glu-PEG-PLL-LA)

Glu-PEG-PLL-LA was synthesized according to the synthetic route shown in Fig. 2A. Briefly, the BIG-PEG-PLL(TFA) was firstly synthesized by ring opening polymerization of Lys(TFA)-NCA with BIG-PEG-NH_2 as a macroinitiator. Degree of polymerization of PLL(TFA) segment (DP_{PLL}) was determined to be 40 in ^{1}H-NMR spectrum (400 MHz, ECS-400, JEOL, Tokyo, Japan) and a molecular weight distribution (M_w/M_n) was determined to be 1.10 in gel permeation chromatography (GPC) (HLC-8220, Tosoh Corporation, Tokyo, Japan) using DMF containing 10 mM LiCl as carrier solvent [45]. The obtained BIG-PEG-PLL(TFA) was reacted with LA-NHS (20 equiv.) and DIPEA (10 equiv.) in DMF at 40 °C for 24 h, followed by dialysis and lyophilization to obtain the BIG-PEG-PLL(TFA)-LA as white powder. The conjugation rate of LA in BIG-PEG-PLL(TFA)-LA was determined to be 80% from the peak intensity ratio of the methylene protons of LA (-CO*CH*$_2$CH$_2$- and -CH*CH*HCH$_2$SS-, 3H, δ = 2.4 ppm) to the ethylene protons of PEG (-(OC*H*$_2$C*H*$_2$)-, 4H, δ = 3.6–3.8 ppm) in ^{1}H-NMR spectra (400 MHz, 40 °C, MeOD) (Fig. S1). Finally, Glu-PEG-PLL-LA was obtained as white powder through deprotection of TFA moieties in the mixture of methanol and 1 N NaOH solution (9:1, v/v) for 8 h at 35 °C, and deprotection of BIG moieties in 90 % TFA for 20 min at room temperature. The complete deprotection of TFA and BIG was confirmed by the peak shifting of methylene protons from 3.3 to 3.0 ppm, and the disappearance of the proton signals of the BIG moiety at 6.0, 6.1, 7.3, and 7.4 ppm from ^{1}H-NMR spectra, respectively (Fig. 2B). Meanwhile, the MeO-PEG-PLL-LA with DP_{PLL} of 40 was synthesized as a control.

2.3. Fluorescence correlation spectroscopy (FCS)

FCS measurements were carried out on a ConfoCor3 module-equipped confocal laser scanning microscope (LSM510, Carl Zeiss, Oberkochen, Germany). The Alexa647-siRNA was excited by a He-Ne laser (633 nm) with the corresponding band-pass filter to filtrate the emission. The Alexa647-siRNA/polymer mixtures having different molar ratios ([polymer]/[siRNA] = 0:1, 0.5:1, 0.75:1, 1:1, 1.25:1, 1.5:1, and 2:1) were prepared in 10 mM HEPES buffer (pH 7.2) containing 150 mM NaCl with the siRNA concentration as 10 nM, followed by 1 h incubation at room temperature. Then, the resulting mixtures were measured

ACCEPTED MANUSCRIPT

using an 8-well Lab-Tek chambered cover-glass (Nalge Nunc International, Rochester, NY, USA) and the diffusion time was averaged from 10 measurements with a sampling time of 10 s. The diffusion coefficient of each sample was converted from diffusion time using Cy5 maleimide (GE Healthcare, UK) as a reference.

2.4. Analytical ultracentrifuge (AUC)

The mixture of [polymer]/[siRNA] = 1 with siRNA concentration of 600 nM was prepared in 10 mM HEPES buffer (pH 7.2) containing 150 mM NaCl, followed by equilibrium sedimentation in an AUC equipped with absorbance optics (Beckman Coulter, Brea, CA, USA) for 3 days. The absorbance at 260 nm was recorded and the MW of uPIC was determined as previously described using ORIGIN software (Beckman Coulter) [39].

2.5. Preparation of Glu-NPs

The Glu-NPs were prepared using a two-step assembling approach (Fig. 1). Glu-PEG-PLL-LA and siRNA were separately dissolved at 15 μM in 10 mM HEPES buffer (pH 7.2) containing 5% sucrose, and then mixed at a molar ratio of 1:1 to form uPIC. Then, the uPIC solution was added to an AuNP solution (0.15 mM) containing 5% sucrose at a molar ratio of uPIC:AuNP = 500:1, followed by 12 h incubation at 4 °C. Then, NaCl was added to the mixed solution to improve the uPIC conjugation efficiency (final NaCl concentration: 150 mM). After 24 h incubation with NaCl, the uPIC-coated AuNPs were further treated with 30 μM PEG-SH (MW: 800) for 24 h at 4 °C, purified by centrifugation (20,400 g, 20 min), and finally suspended in 10 mM HEPES buffer (pH 7.2) containing 150 mM NaCl and 5% sucrose. Similarly, the MeO-NPs were prepared as a control using MeO-PEG-PLL-LA, instead of Glu-PEG-PLL-LA.

2.6. Size, zeta-potential, UV-visible spectroscopy, and grated PEG-SH amount measurements

Sizes and their distribution of nanoparticles were determined by dynamic light scattering (DLS) using a Zetasizer Nano ZS instrument (Malvern Instrument Ltd., UK) with an incident light (633 nm) and a detection angle of 173° at 25 °C. The corresponding hydrodynamic diameter and polydispersity index (PDI) were analyzed using the cumulant method. The same instrument was employed to test zeta-potentials of nanoparticles using a disposable capillary cell (DTS1070, Malvern Instrument) at 25 °C. The UV-visible spectroscopy (UV-Vis) was obtained from a Spark 20M multimode microplate reader (TECAN, Switzerland). All the samples used for DLS, zeta-potential, and UV-Vis measurements were adjusted to 10 nM AuNPs. The concentration of nanoparticles in bare AuNP, Glu-NP, or MeO-NP solutions was determined by surface plasmon resonance absorbance of nanoparticles in UV-Vis spectra (520 nm for bare AuNP and 528 nm for MeO- and Glu-NPs). For quantification of grafted PEG-SH content per nanoparticle, uPIC-coated AuNPs (20 nM, 40 μL) were incubated with PEG-SH (1.2 mM, 10 μL) at 4 °C for 24 h [40]. The samples were centrifuged at 20,400 g, and the supernatant (40 μL) was collected. Then, the supernatant (40 μL) was reacted with Ellman's reagent (78 μg/mL in 0.1 M sodium phosphate buffer (pH 8.0) containing 1 mM EDTA, 510 μL) at ambient temperature for 15 min. The UV-Vis absorbance of the reaction solution at 412 nm

ACCEPTED MANUSCRIPT

was measured using the TECAN microplate reader to determine the amount of non-grafted PEG-SH. Then, the content of grafted PEG-SH was calculated by subtracting the amount of non-grafted PEG-SH from the total amount.

2.7. Cell culture

Human breast cancer, MDA-MB-231, cells (European Collection of Authenticated Cell Cultures, UK) were cultured in RPMI 1640 medium containing 10% (v/v) FBS (RPMI 1640/FBS) with 5% CO_2 at 37 °C. For spheroid culture, MDA-MB-231 cells in a serum-free DMEM-F12 medium containing B27 (1×, Thermo Fisher), 20 ng/mL recombinant human epidermal growth factor (EGF) (BD Life Sciences, NJ, USA), and 20 ng/mL recombinant human basic fibroblast growth factor (bFGF) (Thermo Fisher) [46] were seeded in 6-well ultralow attachment plates (Corning, ME, USA) or Cell-able 96-well plates (Toyo Gosei, Japan) with a cell density of 5×10^4 cells/mL. The cells were incubated for 7-10 days to form spheroids, then used for further biological experiments.

2.8. Western blot analysis

MDA-MB-231 adherent and spheroid cells were washed with PBS and then lysed with RIPA buffer (Sigma-Aldrich) containing protease inhibitor cocktail (Sigma-Aldrich) for 30 min at 4 ºC. The lysates were centrifuged at 13,000 g for 20 min and the protein concentration of the supernatant was determined using Bradford reagent (Wako). The proteins (20 μg) in supernatant were separated by using an 8% Bis-Tris gel (Invitrogen, Thermo Fisher) and transferred to PVDF membrane (Bio-Rad, USA). The membrane was incubated in 5% skim milk blocking buffer for 12 h at 4 ºC, followed by 1 h incubation with GLUT1 primary antibodies (#12939, Cell Signaling Technology, MA, USA) and another 1 h incubation with HRP-conjugated secondary antibodies (#7074, Cell Signaling Technology). Beta-actin (#4967, Cell Signaling Technology) was used as an internal control. The protein bands were visualized with ECL Prime Western Blotting Detection reagent (Amersham, Little Chalfont, UK) and chemiluminescent imager (LAS-4000, Fujifilm, Tokyo, Japan).

2.9. In vitro cytotoxicity assay

MDA-MB-231 cells were seeded in 96-well plates (5×10^3 cells/well) and incubated in RPMI 1640/FBS for 24 h. Then, the cells were exposed to fresh medium containing siCont-loaded MeO- or Glu-NPs at siRNA concentrations of 50, 100, 200, and 400 nM for 48 h, respectively. The cells were further incubated with fresh RPMI 1640/FBS (100 μL) containing CCK-8 solution (10 μL) for 1 h, followed by absorbance measurement at 450 nm. To calculate relative cell viability, the absorbance was normalized to that from non-treated cells.

2.10. In vitro cellular uptake by flow cytometry

MDA-MB-231 adherent (5×10^4 cells/well, 24-well plate) or spheroid (5×10^4 cells) cells were incubated with Alexa647-siRNA-loaded MeO- or Glu-NPs (siRNA concentration: 100 nM) for 1 h and 4 h. Then, the adherent or spheroid cells were dispersed using trypsin or Accutase cell detachment solutions (Innovative Cell Technologies, CA, USA), respectively, followed by

ACCEPTED MANUSCRIPT

wash with fresh media and suspension in cold PBS. The mean fluorescence intensity of Alexa647-siRNA in the cells was measured by a flow cytometer, BD LSR II (BD Biosciences, San Jose, CA, USA), equipped with 633-nm laser and bandpass filter 660/20. The non-treated cells were used as background. To inhibit the GLUT activity, the spheroids (5×10^4 cells) were incubated with phloretin (concentration: 0.2 mM), a well-known GLUT inhibitor, for 30 min before exposure to the siRNA-loaded nanocarriers. The internalized Alexa647-siRNA within cells was measured by a flow cytometer.

To investigate cellular uptake in highly aldehyde dehydrogenase (ALDH)-expressing ($ALDH^{high}$) cells, an ALDEFLUOR kit (STEMCELL Technology, Vancouver, BC, Canada) was used to identify the $ALDH^{high}$ cells. The spheroids (1×10^6 cells) were incubated with Alexa647-siRNA-loaded MeO- or Glu-NPs (siRNA concentration: 100 nM) for 1 h and dispersed into single cells using Accutase cell detachment solutions. The suspended cells were stained with the ALDEFLUOR kit based on the manufacturer's instruction and measured by BD LSR II. The data were analyzed by FlowJo software.

2.11. In vitro confocal laser scanning microscopic (CLSM) observation

MDA-MB-231 spheroids (5×10^4 cells) were incubated with media containing Alexa647-siRNA-loaded MeO- or Glu-NPs (siRNA concentration: 100 nM) for 4 h. Then, the spheroids were washed with fresh medium, stained with Hoechst 33342, and imaged with CLSM using a Zeiss LSM 510 (Carl Zeiss, Germany).

2.12. In vitro gene silencing assay by quantitative real-time PCR (qRT-PCR)

MDA-MB-231 adherent (5×10^4 cells/well, 24-well plate) and spheroid (5×10^4 cells) cells were incubated with siPLK1 or siCont-loaded MeO- or Glu-NPs (siRNA concentration: 50, 100, and 200 nM) for 48 h. Then, the total RNA was extracted using RNeasy MiNi Kit (Qiagen, Valencia, CA, USA) according to the manufacturer's instruction. The extracted RNA samples were diluted to the same concentration (20 μg/μL), followed by reverse transcription from RNA to cDNA using ReverTra Ace (Toyobo, Osaka, Japan). The qRT-PCR was carried out using TaqMan gene expression assay protocol with an ABI 7500 fast real-time PCR system (Applied Biosystems, Foster City, CA, USA). The human beta-actin probe was employed as an endogenous house-keeping gene to normalize the PLK1 mRNA amount. The mRNA expression level was calculated based on comparative $2^{-\Delta\Delta Ct}$ method and normalized to that obtained from non-treated cells [47]. Results are expressed as mean and standard deviation (n = 4).

2.13. Orthotopic xenograft tumor model

To establish an MDA-MB-231 orthotopic breast tumor model, 5×10^6 MDA-MB-231 cells in 100 μL DMEM-F12/Matrigel (1:1, v/v) were inoculated to the mammary fat pad of NOD/SCID mice or BALB/c nude mice (female, 8 weeks old). The *in vivo* biodistribution, gene silencing efficacy, and antitumor activity studies were performed when the tumor volumes reached to approximately 100, 100, and 50 mm^3, respectively.

2.14. In vivo tumor accumulation and biodistribution of Glu-NPs

ACCEPTED MANUSCRIPT

The tumor accumulations of MeO- and Glu-NPs were studied by the fluorescence of dye-labeled siRNA. Alexa647-siRNA-loaded MeO- or Glu-NPs were intravenously injected into the tail vein of the MDA-MB-231 tumor-bearing BALB/c nude mice (5 μg siRNA/mouse, n = 3). The mice were sacrificed at 24 h post injection. The tumor tissues were collected, homogenized, and incubated in lysis buffer containing 120 mM 2-mercaptoethanol for 12 h at 4 ºC. A Spark 20M multimode microplate reader was employed to quantify the relative accumulation of MeO- and Glu-NPs in tumor tissues by measuring the fluoresce intensity of Alexa647-siRNA. Results are expressed as mean and standard deviation (n = 3).

An inductively coupled plasma mass spectrometry (ICP-MS) was employed to determine the biodistribution profiles of MeO-NP and Glu-NP by measuring the content of Au. siCont-loaded MeO-NP or Glu-NP were intravenously injected into the tail vein of the BALB/c nude mice (5 μg siRNA/mouse, n = 3). The mice were sacrificed at 1, 4, and 24 h post injection, followed by collection and homogenization of major organs. The homogenized organs were decomposed with nitric acid on a hot plate. The dried samples were suspended in aqua regia, diluted in 1% HNO_3 solution, and filtered using a 0.45 μm pore size membrane filter before quantification of Au content using an Agilent 7700 ICP-MS system (Agilent, CA, USA). Results are expressed as mean and standard deviation (n = 3).

2.15. In vivo gene silencing efficacy of Glu-NPs

The siCont-loaded MeO- and Glu-NPs, and siPLK1-loaded MeO- and Glu-NPs were intravenously injected into the MDA-MB-231 tumor-bearing BALB/c nude mice from tail vein (20 μg siRNA/injection/mouse, 4 injections) at 48, 72, 96, and 120 h before collection of tumors (n = 4). The mice injected with saline (200 μL/injection) using the same injection protocol were employed as controls. Tumor tissues were excised and homogenized by using an ultrasonic disruptor (UR-20P, Tomy Seiko, Co., Ltd., Tokyo, Japan). Total mRNA was extracted by using RNeasy MiNi Kit. Thereafter, the relative PLK1 mRNA amounts in the tumor tissues were quantified by qRT-PCR as described above.

2.16. In vivo tumor growth inhibition activity

The MDA-MB-231 tumor-bearing NOD/SCID mice were randomly divided into 4 groups (n = 5). Then, the tumor-bearing mice were treated with saline, siCont-loaded Glu-NPs, and siPLK1-loaded MeO- and Glu-NPs by intravenous injection to the tail vein (20 μg siRNA/injection) on day 0, 1, 4, 5, 8, 9, 12 and 13. Tumor sizes were monitored by a caliper every other day, and the tumor volume was calculated based on the following equation: tumor volume = 0.5 × (major diameter) × (minor diameter)^2.

2.17. Analysis of the proportion of CSCs in tumor

At the final day of tumor growth inhibition study, the mice were sacrificed and the tumor tissues were excised. The excised tumor tissues were immediately transferred to cold DMEM-F12 medium, cut into small pieces, and suspended in 20 mL cold DMEM-F12 medium, followed by centrifuge for 5 min at 150 g at 4 ℃. The pellet was further digested in 10 mL Accumax/EDTA tissue dissociation solution (Innovative Cell Technologies) at room

ACCEPTED MANUSCRIPT

temperature for 30 min on a shaker. The tumor cells were collected by centrifuge and filtration through a 200-mesh sieve, stained with ALDEFLUOR kit, and measured by a flow cytometer. The data were analyzed by FlowJo software, and the results are expressed as mean and standard deviation (n = 3).

2. 18. Blood toxicity assays

BALB/c mice (female, 6-week old) were intravenously injected with one or four injection(s) of either Glu-NP (20 μg siRNA/shot) or saline. Four injections were performed at 24 h intervals. At 7 days after the first injection, the mice were anesthetized with isoflurane and the blood (180 μL) was collected from posterior vena cava using 23G needles. The numbers of white blood cells (WBC), red blood cells (RBC), and platelets (PLT) in the collected blood samples were determined using an automated hematology analyzer (pocH-100iV Diff, Sysmex Corporation, Hyogo, Japan).

2.19. Statistical analysis

The experimental data were analyzed by a two-tailed Student's t-test in Microsoft Excel. The * and ** indicate $p < 0.05$ and $p < 0.01$, respectively, and were considered to be statistically significant.

3. **Results and discussion**

3.1. Synthesis of Glu-PEG-PLL-LA

To construct Glu-NPs, the glucose-conjugated block copolymer, Glu-PEG-PLL-LA, was synthesized to contain a glucose moiety on the α-terminal of PEG, a PLL segment with 40 units, and a LA disulfide moiety on the ω-terminal of PLL that was constrained to a narrow molecular weight distribution (M_w/M_n = 1.10) (Fig. 2A). Following a previously established ring-opening polymerization of ethylene oxide initiated by protected glucose [42], the Glu ligand was quantitatively introduced to the PEG end through ether linkage at the C6 position. In this way, the OH groups at the C1, C3, and C4 positions remain intact, allowing for the effective recognition by GLUT1 [41, 48]. Importantly, the DP_{PLL} of 40 ensured the formation of uPIC between a single block copolymer with 40 positive charges (pK_a = 9.54) and a single siRNA with 40 negative charges through charge-matched PIC formation [49]. Furthermore, the LA disulfide moiety served as a coordinate linkage between the uPICs and AuNP. In the similar way, the MeO-PEG-PLL-LA without Glu ligand was also synthesized to construct non-targeted MeO-NPs as a control.

ACCEPTED MANUSCRIPT

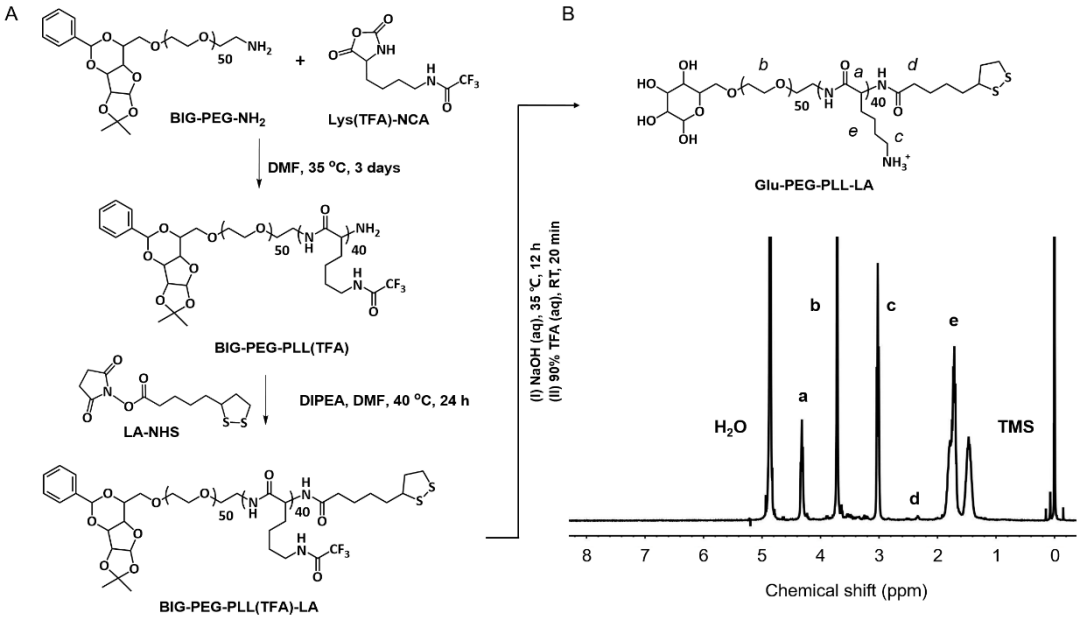

Fig. 2. (A) Synthetic route of Glu-PEG-PLL-LA. (B) ^{1}H-NMR spectrum of Glu-PEG-PLL-LA (400 MHz, polymer concentration: 10 mg/mL, temperature: 25 °C, solvent: D_2O).

3.2. Preparation of Glu-NPs

A two-step nanoconstruction was employed for preparing Glu-NPs, which consisted of the formation of monodispersed uPICs followed by the monolayer conjugation of uPICs onto the AuNP surface. The formation of uPICs between Glu-PEG-PLL-LA (or MeO-PEG-PLL-LA) and siRNA was validated by FCS and AUC [49]. The FCS results show that the diffusion coefficient of block copolymer (or Polymer) and Alexa647-siRNA PICs had the lowest value at a molar ratio of [Polymer]/[siRNA] = 1, with unchanged values at molar ratios > 1 (Fig. S2), which indicates that the siRNA and polymer formed a 1:1 PIC solution. Furthermore, the AUC data demonstrate that the MW of the PIC was comparable to the total MW of a single molecular pair between the block copolymer and siRNA (Table S1), consistent with the formation of a 1:1 uPIC solution. The approximately similar FCS results between Glu-PEG-PLL-LA and MeO-PEG-PLL-LA indicate that glucose ligand installation did not affect uPIC formation. The obtained uPICs were then further conjugated onto the AuNPs through Au-S coordinate bonds in the presence of sucrose. The conjugation was confirmed using UV-visible spectroscopy (UV-Vis), with a red shift of the AuNP absorbance observed after the conjugation reaction (Fig. 3A). The DLS and zeta-potential measurements further indicated the successful uPIC-coating of AuNPs as increases in both the hydrodynamic diameter and zeta-potential of AuNPs were clearly observed after uPIC conjugation (Fig. 3B and Table 1). It is noted that the addition of sucrose to buffer was essential to construct the Glu-NPs with a size of less than 50 nm. This was probably due to the inhibition of hydrogen bonding between glucoses on the AuNP surfaces (Table S2). The numbers of uPIC on each AuNP were determined to be ca. 65 based on the fluorescence intensity of Alexa647-siRNA. Meanwhile, the backfilled PEG-SH (M_w = 800)

ACCEPTED MANUSCRIPT

amount was measured to be ca. 2800 based on the absorbance derived from Ellman's reagent, which provided more neutral zeta-potential of uPIC-AuNPs [40] (Table 1). The unique Glu-NP structure has several advantages: (1) Glu-mediated targetability to GLUT1, (2) PEG-derived stealthiness, and (3) a uniform sub-50-nm size.

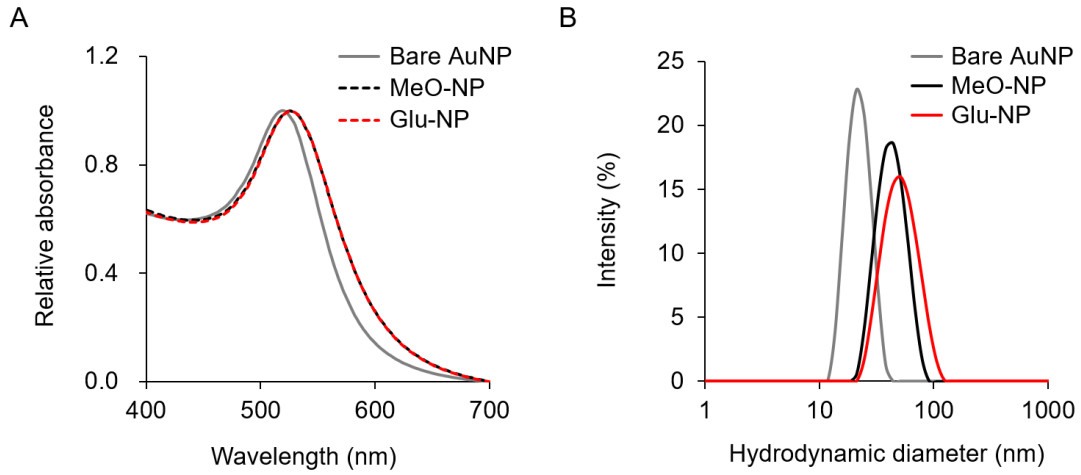

Fig. 3. (A) UV-Vis spectra of bare AuNP, MeO-NP, and Glu-NP. (B) Intensity-based DLS histograms of bare AuNP, MeO-NP, and Glu-NP.

Table 1. Physicochemical properties of bare AuNP, MeO-NP, and Glu-NP.

Sample	Size (nm)[a]	PDI[a]	Zeta-potential (mV)[b]	Capped siRNA	Grafted PEG[c]
Bare AuNP	20	0.04	–30.4 ± 1.0	0	0
MeO-NP	40	0.10	–15.8 ± 0.8	66 ± 4	2810 ± 210
Glu-NP	47	0.15	–16.8 ± 0.7	65 ± 3	2970 ± 410

[a]Hydrodynamic diameter and polydispersity index (PDI) were determined by DLS.
[b]Zeta-potential was measured in 10 mM HEPES buffer (pH 7.2) without NaCl.
[c]Grafted amount of PEG-SH (M_W: 800) was determined using Ellman's reagent.

3.3. In vitro Glu-NP cellular uptake against MDA-MB-231 spheroid cell cultures

MDA-MB-231 cells were reported to overexpress mainly GLUT1 on their surface due to the Warburg effect [50-54] compared to other breast cancer cells, *e.g.*, MCF-7 and MDA-MB-435 [51], suggesting that they are potential targets of glucose-conjugated nanoparticles. MDA-MB-231 cells express an extremely high level of GLUT1 with negligible levels of GLUT2, GLUT3, GLUT4, and GLUT5 [51, 55]. Thus, Glu-NP was more likely uptaken by MDA-MB-231 cells through binding to GLUT1 rather than the other GLUT isoforms. This fact motivated us to examine the cellular uptake of Glu-NPs in cultured MDA-MB-231 cells. First, the cellular uptake profiles in adherent cells were compared between Glu-NPs and MeO-NPs incorporating Alexa647-siRNA (Fig. S3). The cells treated with

ACCEPTED MANUSCRIPT

Glu-NPs displayed significantly higher fluorescence intensities compared with those treated with MeO-NPs, indicating that the Glu ligands enhanced the cellular uptake of uPIC-AuNPs. Note that the modest cellular uptake of Alexa647-siRNA was observed for MeO-NPs without Glu ligands, probably due to the nonspecific adsorptive endocytosis. This relies on the stable conjugation of uPICs with AuNP, making MeO-NPs tolerable upon the adsorption process on the cellular surface coated with anionic glycocalyx [39].

The cellular uptake of Glu-NPs was then investigated in a spheroid culture of MDA-MB-231 cells since the spheroid culture is more relevant to an *in vivo* 3D cancer cell condition in terms of the gene expression pattern as well as the accessibility of nanoparticles [56]. Furthermore, the spheroid culture is regarded as a convenient method to evaluate CSC functions because a hypoxic condition within the spheroid is more favorable for CSC growth [57]. A higher expression of ALDH, which is a CSC marker, was observed for the spheroid culture of MDA-MB-231 cells, compared with their adherent culture (Fig. S4). In parallel, the GLUT1 expression level was also increased in the spheroid culture (Fig. S5), probably due to enhanced glycolytic CSC activity [20, 58, 59]. Of note, a positive correlation between GLUT1 expression and ALDH activity was observed in MDA-MB-231 cells, particularly in the spheroid culture (Fig. S6). We, therefore, assumed that Glu-NPs should more effectively bind to the spheroid cancer cells, especially to CSCs, due to their higher GLUT1 expression. The cellular uptake efficiency of Glu-NPs was compared with MeO-NPs in both the presence and absence of phloretin as a GLUT inhibitor (Fig. 4A). The Glu-NPs exhibited higher cellular uptake efficiency than the MeO-NPs in the absence of phloretin, as higher fluorescence intensity was observed for the cells treated with Glu-NPs. This enhanced cellular uptake efficiency was eliminated when the spheroids were treated with phloretin, indicating that the enhanced cellular uptake of Glu-NPs was attributed to the specific interaction between Glu ligands and GLUT1. The increasing cellular uptake of Glu-NPs was also confirmed by CLSM observations (Fig. 4B). The ALDEFLUOR kit was employed to further clarify the targetability of Glu-NPs to CSCs and identify the cellular internalizations of $ALDH^{high}$ cells and $ALDH^{normal}$ cells in the spheroids (Fig. 4C). While the cellular uptake of Glu-NPs was higher in both $ALDH^{high}$ cells and $ALDH^{normal}$ cells compared with that of MeO-NPs, larger enhancements in the cellular uptake of Glu-NPs were discovered in the $ALDH^{high}$ cells (1.7-fold enhancement for MeO-NPs) compared with that in the $ALDH^{normal}$ cells (1.4-fold enhancement for MeO-NPs). These results indicate that the Glu-NPs enabled GLUT1-mediated active targeting of the breast cancer MDA-MB-231 cells, particularly the CSC (or $ALDH^{high}$ cell) fraction. Of note, the higher cellular uptake of MeO-NP was also observed in $ALDH^{high}$ cells, compared with $ALDH^{normal}$ cells, although the level of the uptake was significantly lower than the case observed for Glu-NP. It is reported that CSCs undergo metabolic alterations and exhibit higher glycolytic activity than normal cancer cells [9, 18]. Presumably, the elevated metabolism of CSCs ($ALDH^{high}$ cells) might also activate the non-specific cellular uptake of MeO-NP.

ACCEPTED MANUSCRIPT

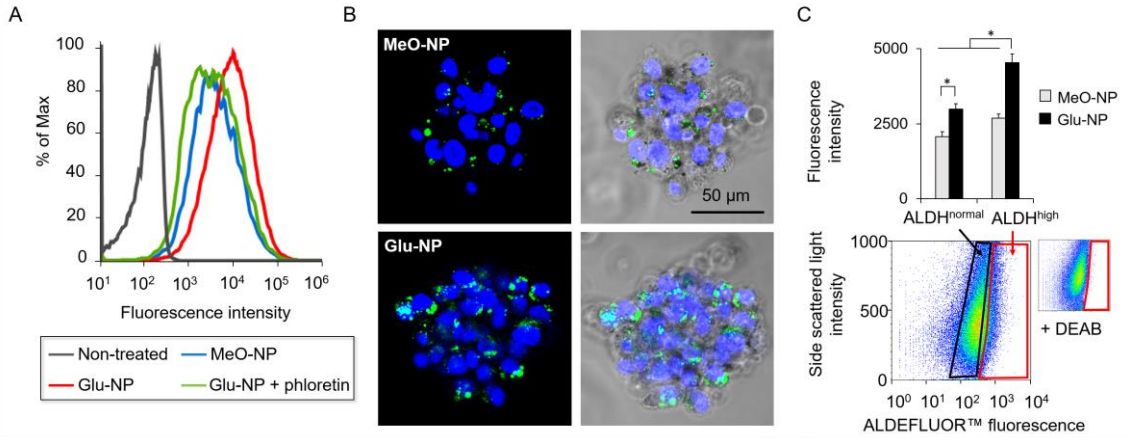

Fig. 4. (A) Degree of MeO- and Glu-NP cellular uptake in MDA-MB-231 cell spheroids, determined by flow cytometry. The spheroids were incubated with Alexa647-siRNA-loaded MeO-NPs (blue line), Glu-NPs (red line), and a mixture of Glu-NPs and phloretin (0.2 mM) (green line) for 1 h (siRNA concentration: 100 nM). (B) CLSM images of the MDA-MB-231 cell spheroids treated with Alexa647-siRNA-loaded MeO- and Glu-NPs (siRNA concentration: 100 nM) for 4 h. (C) *In vitro* cellular uptake of MeO- and Glu-NPs in $ALDH^{high}$ and $ALDH^{normal}$ cells (siRNA concentration: 100 nM). The cells treated with *N*,*N*-diethylaminobenzaldehyde (DEAB), an ALDH inhibitor, were employed to determine the $ALDH^{high}$ cell fraction. Results are expressed as mean and standard deviation (n = 3, $*p < 0.05$).

3.4. In vitro gene silencing activity of Glu-NPs

The silencing ability of Glu-NPs for PLK1 gene was studied in both adherent and spheroid cultures of MDA-MB-231 cells by qRT-PCR. The inhibition of PLK1 expression is proven to be a potential strategy to suppress the proliferation of cancer cells because PLK1 plays an important role in the cell cycle of cancer cells [60]. The siPLK1-loaded Glu-NPs exhibited significantly higher gene silencing efficiencies in both adherent cells and spheroids in a sequence-specific manner (Fig. 5), demonstrating that the Glu ligands enhanced the gene silencing activity of uPIC-AuNPs by facilitating cellular uptake. It should be noted that the Glu-NP gene silencing efficiency was higher in spheroid cells compared with that in adherent cells, with 77% knockdown in the spheroids compared with 52% knockdown in the adherent cells at 200 nM siRNA. The enhanced Glu-NP gene silencing efficiency in the spheroid culture may result from the higher GLUT1 expression level, which allows enhanced cellular uptake of Glu-NPs, since the gene silencing efficiency of MeO-NPs was not altered between the adherent and spheroid cultures. Furthermore, Glu-NPs progressively (or linearly) increased the gene silencing efficiency up to 77% knockdown with an increase in siRNA concentration, whereas the gene silencing efficiency of MeO-NPs was apparently saturated at around 25% knockdown (Fig. S7). This result suggests that the GLUT1-mediated endocytosis might have larger capacity for nanoparticle internalization compared with nonspecific adsorptive endocytosis. It should also be noted that both Glu-NPs and MeO-NPs showed minimal cytotoxicity in MDA-MB-231 cells for siRNA concentration up to 400 nM (Fig. S8).

ACCEPTED MANUSCRIPT

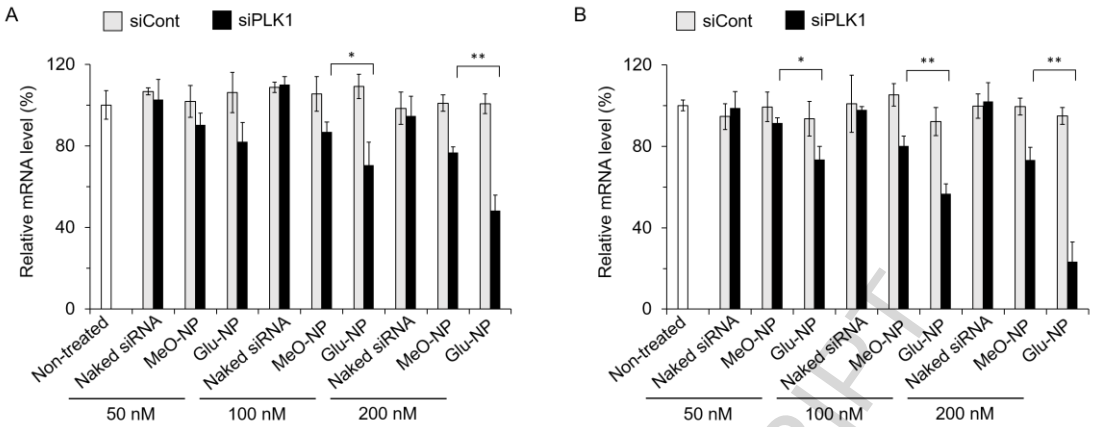

Fig. 5. *In vitro* PLK1 gene silencing efficiencies of MeO- and Glu-NPs in (A) MDA-MB-231 adherent cells and (B) spheroid cells. The adherent or spheroid cells were incubated with siPLK1-loaded MeO- and Glu-NPs for 48 h (siRNA concentration: 50, 100, and 200 nM), followed by qRT-PCR. All results are expressed as mean and standard deviation (n = 4, *$p < 0.05$ and **$p < 0.01$).

3.5. In vivo performances of Glu-NPs

To clarify *in vivo* behaviors of Glu-NPs, the tumor accumulation and gene silencing efficiencies of Glu-NPs were examined in an orthotopic MDA-MB-231 tumor-bearing mouse model. The tumor accumulation of Alexa647-siRNA delivered by Glu-NPs was significantly higher than that by MeO-NPs at 24 h post injection (Fig. 6A), which demonstrates the enhanced tumor-targetability of Glu-NPs. Note that remarkable differences were not observed between MeO-NP and Glu-NP in their biodistribution profiles in major healthy organs (Fig. S9). The similar profiles between MeO-NP and Glu-NP are apparently consistent with those reported in the previous studies developing GLUT1-targeted NPs [41, 61]. This might be due to relatively lower density of GLUT1 (or GLUT family) on the luminal plasma membrane in healthy organs, compared with MDA-MB-231 cells. The lower density of GLUT1 is more difficult to generate the significant multivalent binding to Glu-NP, which may be required for the GLUT1 targeting by Glu to compensate their relatively low Michaelis constant (*i.e.*, K_m: 3 mmol/L) [54]. In this regard, the brain capillary endothelial cells (BCECs) are reported to express a high degree of GLUT1 [62]. The considerably low level of brain accumulation of Glu-NPs, as well as MeO-NPs, might be explained by two possible mechanisms; i) the effective transcytosis of Glu-NP into the brain tissue might not occur; and ii) the GLUT1 density on the luminal plasma membrane of BCECs might not be sufficiently high in the normal glycemic condition because it is significantly affected by the plasma glucose level [62]. Furthermore, the siPLK1-loaded Glu-NPs displayed significantly higher gene silencing efficiency in the tumor tissues compared with the siPLK1-loaded MeO-NPs in a sequence-specific manner (Fig. 6B). The antitumor efficacy of siPLK1-loaded Glu-NPs was also evaluated for the same tumor model. The tumor-bearing mice were randomly divided into four groups (n = 5), with each group receiving intravenous administration of either a saline, siCont-loaded Glu-NPs, siPLK1-loaded MeO-NPs, or siPLK1-loaded Glu-NPs multi-dose treatment at 20 μg siRNA/injection/mouse. The tumor

ACCEPTED MANUSCRIPT

growth profiles indicated that the mice treated with siPLK1-loaded Glu-NPs exhibited the slowest tumor growth rate among the tested formulations (Fig. 6C). The relative tumor volume in the mice treated with siPLK1-loaded Glu-NPs (6.9 ± 1.3) was significantly smaller than those treated with siPLK1-loaded MeO-NPs (10.8 ± 2.1) 28 days after the first injection, which demonstrates the enhanced antitumor efficacy of Glu-NPs. However, there were no significant alterations in mouse body weight during the treatment, indicating negligible systemic toxicity of both the MeO- and Glu-NPs (Fig. 6D). Then, the change in the CSC (or $ALDH^{high}$ cell) proportion in tumors was examined (Fig. 6E). Note that the $ALDH^{high}$ population in saline-treated tumors as control was similarly determined to be those reported in the previous studies [6, 63, 64]. The CSC (or $ALDH^{high}$ cell) proportion in the tumors treated with siPLK1-loaded Glu-NPs was significantly lower than that treated with saline, siCont-loaded Glu-NPs, and siPLK1-loaded MeO-NPs, probably due to the preferential accumulation of Glu-NPs in the CSCs and their RNAi-driven anticancer effect. In addition, there were no significant differences in the levels of WBC, RBC, and PLT between Glu-NP-treated mice and saline-treated mice even after 4 doses (Fig. S10), indicating negligible hematological toxicity of Glu-NP under the tested condition

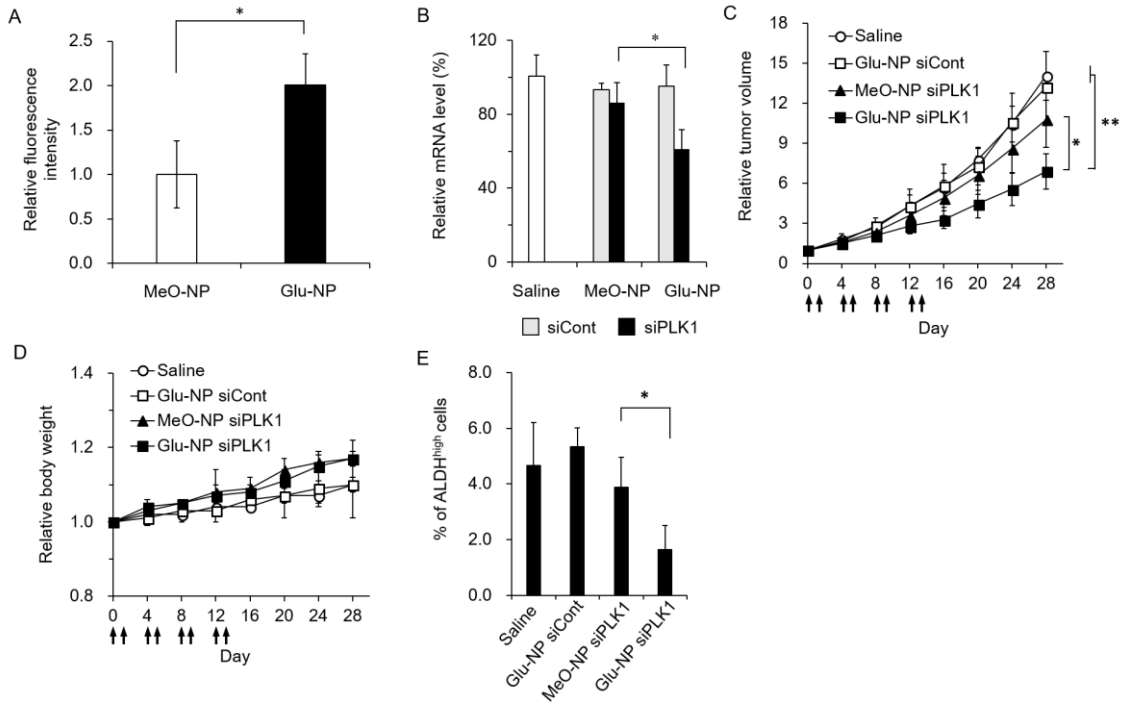

Fig. 6. *In vivo* Glu-NP performances in MDA-MB-231 orthotopic tumor model. (A) Relative tumor accumulation of Alexa647-siRNA-loaded MeO- and Glu-NPs at 24 h post intravenous administration (5 μg siRNA/mouse, n = 3). (B) PLK1 mRNA levels in the MDA-MB-231 tumor tissues after treatment with MeO- and Glu-NPs (n = 4). The siRNA-loaded samples (20 μg siRNA/injection/mouse, 4 injections) were intravenously injected into the mouse tail vein at 48, 72, 96, and 120 h before tumor excision. (C) Tumor growth profiles of the tumor-bearing mice treated with saline, siCont-loaded Glu-NPs, siPLK1-loaded MeO-NPs, and siPLK1-loaded

ACCEPTED MANUSCRIPT

Glu-NPs (20 μg siRNA/injection/mouse, 8 injections) (n = 5). (D) Relative body weights of the mice during the tumor growth inhibition study. (E) The proportion of $ALDH^{high}$ cells in the tumor tissues at day 28 in the tumor growth inhibition study (n = 3). The arrows in (C) and (D) indicate the days when intravenous administration of samples occurred. All results are expressed as mean and standard deviation (*$p < 0.05$ and **$p < 0.01$).

4. Conclusions

The present study demonstrates that Glu-NP is an efficient nanocarrier for delivering therapeutic siRNA to the CSC-rich orthotopic breast cancer model via a systemic route. The Glu-NPs facilitated the cellular uptake of siRNA payloads into GLUT1-overexpressing MDA-MB-231 cell spheroids due to the specific interaction between the Glu ligands and GLUT1. The Glu-NPs displayed enhanced gene silencing activity and improved antitumor efficacy in the MDA-MB-231 orthotopic tumor via intravenous administration compared with the control MeO-NPs. It is particularly noted that the Glu-NPs were able to efficiently reduce the CSC ($ALDH^{high}$ cell) proportion in the orthotopic tumors. It is, therefore, expected that the Glu-NPs that can largely remove the CSCs would achieve high efficacy for cancer ablation with the assistance of cytotoxic anticancer agents to eliminate the differentiated cancer cells. This work demonstrates the potential of employing Glu-installed nanomedicines for efficient tumor treatment by targeting CSCs in tumors, therefore providing a promising platform technology for targeted siRNA delivery to achieve successful RNAi-based cancer therapy.

Acknowledgments

This work was financially supported by Center of Innovation (COI) program from Japan Science and Technology Agency (JST) and Grants-in-Aid for Scientific Research (KAKENHI Grant Numbers 25000006 and 18H04170 for KK, 25282141 and 17H02098 for KM, and 18K18378 for HJK) from Ministry of Education Culture, Sports, Science and Technology (MEXT). This work was also partially supported by the Project for Cancer Research and Therapeutic Evolution (P-CREATE) and Basic Science and Platform Technology Program for Innovative Biological Medicine from Japan Agency for Medical Research and Development (AMED), and a grant JSPS Core-to-Core Program, A. Advanced Research Networks. The authors thank Mr. S. Fukushima for his help in polymer syntheses and Ms. S. Ogura for her assistance in animal experiments.

Data availability

The raw/processed data required to reproduce these findings are available from the authors upon request.

References

[1] C. Allemani, T. Matsuda, V. Di Carlo, R. Harewood, M. Matz, M. Nikšić, et al., Global surveillance of trends in cancer survival 2000–14 (CONCORD-3): analysis of individual records for 37 513 025 patients diagnosed with one of 18 cancers from 322 population-based registries in 71 countries, The Lancet 391 (2018) 1023-1075.

ACCEPTED MANUSCRIPT

[2] Q. Pan, Q. Li, S. Liu, N. Ning, X. Zhang, Y. Xu, A.E. Chang, M.S. Wicha, Concise review: targeting cancer stem cells using immunologic approaches, Stem Cells 33 (2015) 2085-2092.
[3] H. Clevers, The cancer stem cell: premises, promises and challenges, Nat. Med. 17 (2011) 313-319.
[4] S. Shen, J. Xia, J. Wang, Nanomedicine-mediated cancer stem cell therapy, Biomaterials 74 (2016) 1-18.
[5] N. Takebe, L. Miele, P.J. Harris, W. Jeong, H. Bando, M. Kahn, S.X. Yang, S.P. Ivy, Targeting Notch, Hedgehog, and Wnt pathways in cancer stem cells: clinical update, Nat. Rev. Clin. Oncol. 12 (2015) 445-464.
[6] H. Kinoh, Y. Miura, T. Chida, X. Liu, K. Mizuno, S. Fukushima, Y. Morodomi, N. Nishiyama, H. Cabral, K. Kataoka, Nanomedicines eradicating cancer stem-like cells in vivo by pH-triggered intracellular cooperative action of loaded drugs, ACS Nano 10 (2016) 5643-5655.
[7] J. Zhang, H. Kinoh, L. Hespel, X. Liu, S. Quader, J. Martin, T. Chida, H. Cabral, K. Kataoka, Effective treatment of drug resistant recurrent breast tumors harboring cancer stem-like cells by staurosporine/epirubicin co-loaded polymeric micelles, J. Control. Release 264 (2017) 127-135.
[8] V. Plaks, N. Kong, Z. Werb, The cancer stem cell niche: how essential is the niche in regulating stemness of tumor cells? Cell Stem Cell 16 (2015) 225-238.
[9] A. Deshmukh, K. Deshpande, F. Arfuso, P. Newsholme, A. Dharmarajan, Cancer stem cell metabolism: a potential target for cancer therapy, Mol. Cancer 15 (2016) 69.
[10] R. Sun, Y. Liu, S. Li, S. Shen, X. Du, C. Xu, Z. Cao, Y. Bao, Y. Zhu, Y. Li, X. Yang, J. Wang, Co-delivery of all-trans-retinoic acid and doxorubicin for cancer therapy with synergistic inhibition of cancer stem cells, Biomaterials 37 (2015) 405-414.
[11] A. Mokhtarzadeh, S. Hassanpour, Z.F. Vahid, M. Hejazi, M. Hashemi, J. Ranjbari, M. Tabarzad, S. Noorolyai, M. de la Guardia, Nano-delivery system targeting to cancer stem cell cluster of differentiation biomarkers, J. Control. Release 266 (2017) 166-186.
[12] W. Alshaer, H. Hillaireau, J. Vergnaud, S. Ismail, E. Fattal, Functionalizing liposomes with anti-CD44 aptamer for selective targeting of cancer cells, Bioconjug. Chem. 26 (2015) 1307-1313.
[13] A. Aires, S.M. Ocampo, B.M. Simoes, M. Josefa Rodriguez, J.F. Cadenas, P. Couleaud, K. Spence, A. Latorre, R. Miranda, A. Somoza, R.B. Clarke, J.L. Carrascosa, A.L. Cortajarena, Multifunctionalized iron oxide nanoparticles for selective drug delivery to CD44-positive cancer cells, Nanotechnology 27 (2016) 065103.
[14] K. Miyano, H. Cabral, Y. Miura, Y. Matsumoto, Y. Mochida, H. Kinoh, C. Iwata, O. Nagano, H. Saya, N. Nishiyama, K. Kataoka, T. Yamasoba, cRGD peptide installation on cisplatin-loaded nanomedicines enhances efficacy against locally advanced head and neck squamous cell carcinoma bearing cancer stem-like cells, J. Control. Release 261 (2017) 275-286.
[15] T.M. Allen, Ligand-targeted therapeutics in anticancer therapy, Nat. Rev. Cancer 2 (2002) 750-763.
[16] A.D. Keefe, S. Pai, A. Ellington, Aptamers as therapeutics, Nat. Rev. Drug Discov. 9 (2010) 537-550.
[17] M.G. Vander Heiden, L.C. Cantley, C.B. Thompson, Understanding the Warburg effect: the

ACCEPTED MANUSCRIPT

metabolic requirements of cell proliferation, Science 324 (2009) 1029-1033.
[18] M. Peiris-Pages, U.E. Martinez-Outschoorn, R.G. Pestell, F. Sotgia, M.P. Lisanti, Cancer stem cell metabolism, Breast Cancer Res. 18 (2016) 55.
[19] C. Hu, M. Niestroj, D. Yuan, S. Chang, J. Chen, Treating cancer stem cells and cancer metastasis using glucose-coated gold nanoparticles, Int. J. Nanomedicine 10 (2015) 2065-2077.
[20] V. Mamaeva, R. Niemi, M. Beck, E. Ozliseli, D. Desai, S. Landor, T. Gronroos, P. Kronqvist, I.K. Pettersen, E. McCormack, J.M. Rosenholm, M. Linden, C. Sahlgren, Inhibiting notch activity in breast cancer stem cells by glucose functionalized nanoparticles carrying gamma-secretase inhibitors, Mol. Ther. 24 (2016) 926-936.
[21] S.M. Elbashir, J. Harborth, W. Lendeckel, A. Yalcin, K. Weber, T. Tuschl, Duplexes of 21-nucleotide RNAs mediate RNA interference in cultured mammalian cells, Nature 411 (2001) 494-498.
[22] P. Resnier, T. Montier, V. Mathieu, J.P. Benoit, C. Passirani, A review of the current status of siRNA nanomedicines in the treatment of cancer, Biomaterials 34 (2013) 6429-6443.
[23] C. Fellmann, S.W. Lowe, Stable RNA interference rules for silencing, Nat. Cell Biol. 16 (2014) 10-18.
[24] B.M. Putzer, M. Solanki, O. Herchenroder, Advances in cancer stem cell targeting: how to strike the evil at its root, Adv. Drug Deliv. Rev. 120 (2017) 89-107.
[25] U. Lachelt, E. Wagner, Nucleic acid therapeutics using polyplexes: a journey of 50 years (and beyond), Chem. Rev. 115 (2015) 11043-11078.
[26] H. Cabral, K. Miyata, K. Osada, K. Kataoka, Block copolymer micelles in nanomedicine application, Chem. Rev. (2018) DOI: 10.1021/acs.chemrev.8b00199.
[27] S. Rietwyk, D. Peer, Next-generation lipids in RNA interference therapeutics, ACS Nano 11 (2017) 7572-7586.
[28] H.J. Kim, A. Kim, K. Miyata, K. Kataoka, Recent progress in development of siRNA delivery vehicles for cancer therapy, Adv. Drug Deliv. Rev. 104 (2016) 61-77.
[29] F. Pittella, H. Cabral, Y. Maeda, P. Mi, S. Watanabe, H. Takemoto, H.J. Kim, N. Nishiyama, K. Miyata, K. Kataoka, Systemic siRNA delivery to a spontaneous panceatic tumor model in transgenic mice by PEGylated calcium phosphate hybrid micelles, J. Control. Release 178 (2014) 18-24.
[30] Y. Jiang, S. Huo, J. Hardie, X. Liang, V.M. Rotello, Progress and perspective of inorganic nanoparticle-based siRNA delivery systems, Expert Opin. Drug Deliv. 13 (2016) 547-559.
[31] C.A. Mirkin, S.H. Petrosko, Spherical nucleic acids: adding a new dimension to nucleic acids and clinical chemistry, Clin. Chem. 64 (2018) 971-972.
[32] J. Shen, W. Zhang, R. Qi, Z. Mao, H. Shen, Engineering functional inorganic-organic hybrid systems: advances in siRNA therapeutics, Chem. Soc. Rev. 47 (2018) 1969-1995.
[33] J.C. Kaczmarek, P.S. Kowalski, D.G. Anderson, Advances in the delivery of RNA therapeutics: from concept to clinical reality, Genome Med. 9 (2017) 60.
[34] Y. Matsumura, H. Maeda, A new concept for macromolecular therapeutics in cancer chemotherapy: mechanism of tumoritropic accumulation of proteins and the antitumor agent smancs, Cancer Res. 46 (1986) 6387-6392.
[35] H. Cabral, Y. Matsumoto, K. Mizuno, Q. Chen, M. Murakami, M. Kimura, Y. Terada, M.R.

ACCEPTED MANUSCRIPT

Kano, K. Miyazono, M. Uesaka, N. Nishiyama, K. Kataoka, Accumulation of sub-100 nm polymeric micelles in poorly permeable tumours depends on size, Nat. Nanotechnol. 6 (2011) 815-823.

[36] Y. Matsumoto, J.W. Nichols, K. Toh, T. Nomoto, H. Cabral, Y. Miura, R.J. Christie, N. Yamada, T. Ogura, M.R. Kano, Y. Matsumura, N. Nishiyama, T. Yamasoba, Y.H. Bae, K. Kataoka, Vascular bursts enhance permeability of tumour blood vessels and improve nanoparticle delivery, Nat. Nanotechnol. 11 (2016) 533-538.

[37] M.E. Davis, J.E. Zuckerman, C.H. Choi, D. Seligson, A. Tolcher, C.A. Alabi, Y. Yen, J.D. Heidel, A. Ribas, Evidence of RNAi in humans from systemically administered siRNA via targeted nanoparticles, Nature 464 (2010) 1067-1070.

[38] R. Kedmi, N. Veiga, S. Ramishetti, M. Goldsmith, D. Rosenblum, N. Dammes, I. Hazan-Halevy, L. Nahary, S. Leviatan-Ben-Arye, M. Harlev, M. Behlke, I. Benhar, J. Lieberman, D. Peer, A modular platform for targeted RNAi therapeutics, Nat. Nanotechnol. 13 (2018) 214-219.

[39] H.J. Kim, H. Takemoto, Y. Yi, M. Zheng, Y. Maeda, H. Chaya, K. Hayashi, P. Mi, F. Pittella, R.J. Christie, K. Toh, Y. Matsumoto, N. Nishiyama, K. Miyata, K. Kataoka, Precise engineering of siRNA delivery vehicles to tumors using polyion complexes and gold nanoparticles, ACS Nano 8 (2014) 8979-8991.

[40] Y. Yi, H.J. Kim, P. Mi, M. Zheng, H. Takemoto, K. Toh, B.S. Kim, K. Hayashi, M. Naito, Y. Matsumoto, K. Miyata, K. Kataoka, Targeted systemic delivery of siRNA to cervical cancer model using cyclic RGD-installed unimer polyion complex-assembled gold nanoparticles, J. Control. Release 244 (2016) 247-256.

[41] Y. Anraku, H. Kuwahara, Y. Fukusato, A. Mizoguchi, T. Ishii, K. Nitta, Y. Matsumoto, K. Toh, K. Miyata, S. Uchida, K. Nishina, K. Osada, K. Itaka, N. Nishiyama, H. Mizusawa, T. Yamasoba, T. Yokota, K. Kataoka, Glycaemic control boosts glucosylated nanocarrier crossing the BBB into the brain, Nat. Commun. 8 (2017) 1001.

[42] T. Nakamura, Y. Nagasaki, K. Kataoka, Synthesis of heterobifunctional poly(ethylene glycol) with a reducing monosaccharide residue at one end, Bioconjug. Chem. 9 (1998) 300-303.

[43] M. Zheng, Y. Zhong, F. Meng, R. Peng, Z. Zhong, Lipoic acid modified low molecular weight polyethylenimine mediates nontoxic and highly potent in vitro gene transfection, Mol. Pharm. 8 (2011) 2434-2443.

[44] J. Turkevich, P.C. Stevenson, J. Hillier, A study of the nucleation and growth processes in the synthesis of colloidal gold, Discuss. Faraday Soc. 11 (1951) 55-75.

[45] A. Harada, K. Kataoka, Formation of polyion complex micelles in an aqueous milieu from a pair of oppositely-charged block copolymers with poly(ethylene glycol) segments, Macromolecules 28 (1995) 5294-5299.

[46] T. Doerks, R.R. Copley, J. Schultz, C.P. Ponting, P. Bork, Systematic identification of novel protein domain families associated with nuclear functions, Genome Res. 12 (2002) 47-56.

[47] K.J. Livak, T.D. Schmittgen, Analysis of relative gene expression data using real-time quantitative PCR and the 2(-Delta Delta C(T)) method, Methods 25 (2001) 402-408.

[48] J.E.G. Barnett, G.D. Holman, K.A. Munday, Structural requirements for binding to the

ACCEPTED MANUSCRIPT

sugar-transport system of the human erythrocyte, Biochem. J. 131 (1973) 211-221.
[49] K. Hayashi, H. Chaya, S. Fukushima, S. Watanabe, H. Takemoto, K. Osada, N. Nishiyama, K. Miyata, K. Kataoka, Influence of RNA strand rigidity on polyion complex formation with block catiomers, Macromol. Rapid Commun. 37 (2016) 486-493.
[50] S.M. Gallagher, J.J. Castorino, D. Wang, N.J. Philp, Monocarboxylate transporter 4 regulates maturation and trafficking of CD147 to the plasma membrane in the metastatic breast cancer cell line MDA-MB-231, Cancer Res. 67 (2007) 4182-4189.
[51] M. Grover-McKay, S.A. Walsh, E.A. Seftor, P.A. Thomas, M.J. Hendrix, Role for glucose transporter 1 protein in human breast cancer, Pathol. Oncol. Res. 4 (1998) 115-120.
[52] A. Krzeslak, K. Wojcik-Krowiranda, E. Forma, P. Jozwiak, H. Romanowicz, A. Bienkiewicz, M. Brys, Expression of GLUT1 and GLUT3 glucose transporters in endometrial and breast cancers, Pathol. Oncol. Res. 18 (2012) 721-728.
[53] A. Godoy, V. Ulloa, F. Rodríquez, K. Reinicke, A.J. Yañes, L. García Mde, R.A. Medina, M. Carrasco, S. Barberis, T. Castro, F. Martínez, X. Koch, J.C. Vera, M.T. Poblete, C.D. Figueroa, B. Peruzzo, F. Pérez, F. Nualart, Differential subcellular distribution of glucose transporters GLUT1-6 and GLUT9 in human cancer: ultrastructural localization of GLUT1 and GLUT5 in breast tumor tissues, J. Cell. Physiol. 207 (2006) 614-627.
[54] C.C. Barron, P.J. Bilan, T. Tsakiridis, E. Tsiani, Facilitative glucose transporters: implications for cancer detection, prognosis and treatment, Metabolism 65 (2016) 124-139.
[55] C. Marini, B. Salani, M. Massollo, A. Amaro, A.I. Esposito, A.M. Orengo, S. Capitanio, L. Emionite, M. Riondato, G. Bottoni, C. Massara, S. Boccardo, M. Fabbi, C. Campi, S. Ravera, G. Angelini, S. Morbelli, M. Cilli, R. Cordera, M. Truini, D. Maggi, U. Pfeffer, G. Sambuceti, Direct inhibition of hexokinase activity by metformin at least partially impairs glucose metabolism and tumor growth in experimental breast cancer, Cell Cycle 12 (2013) 3490-3499.
[56] D.T. Leong, K.W. Ng, Probing the relevance of 3D cancer models in nanomedicine research, Adv. Drug Deliv. Rev. 79-80 (2014) 95-106.
[57] T. Ishiguro, H. Ohata, A. Sato, K. Yamawaki, T. Enomoto, K. Okamoto, Tumor-derived spheroids: relevance to cancer stem cells and clinical applications, Cancer Sci. 108 (2017) 283-289.
[58] E. Vlashi, C. Lagadec, L. Vergnes, K. Reue, P. Frohnen, M. Chan, Y. Alhiyari, M.B. Dratver, F. Pajonk, Metabolic differences in breast cancer stem cells and differentiated progeny, Breast Cancer Res. Treat. 146 (2014) 525-534.
[59] P. Liu, J. Liao, Z. Tang, W. Wu, J. Yang, Z. Zeng, Y. Hu, P. Wang, H. Ju, R. Xu, P. Huang, Metabolic regulation of cancer cell side population by glucose through activation of the Akt pathway, Cell Death Differ. 21 (2014) 124-135.
[60] K. Strebhardt, A. Ullrich, Targeting polo-like kinase 1 for cancer therapy, Nat. Rev. Cancer 6 (2006) 321-330.
[61] Y. Guo, Y. Zhang, J. Li, Y. Zhang, Y. Lu, X. Jiang, X. He, H. Ma, S. An, C. Jiang, Cell microenvironment-controlled antitumor drug releasing-nanomicelles for GLUT1-targting hepatocellular carcinoma therapy, ACS Appl. Mater. Interfaces 7 (2015) 5444-5453.
[62] I. A. Simpson, N. M. Appel. ,M. Hokari, J. Oki, G. D. Holman, F. Maher, E. M. Koehler-Stec, S. J. Vannucci, Q. R. Smith,Blood-brain barrier glucose transporter: effects of

ACCEPTED MANUSCRIPT

hypo- and hyperglycemia revisited, J. Neurochem. 72 (1999) 238-247.
[63] R. Du, B. Liu, L. Zhou, D. Wang, X. He, X. Xu, L. Zhang, C. Niu, S. Liu, Downregulation of annexin A3 inhibits tumor metastasis and decreases drug resistance in breast cancer, Cell Death. Dis. 9 (2018) 126.
[64] H. Lu, D. Samanta, L. Xiang, H. Zhang, H. Hu, I. Chen, J. W. Bullen, G. L. Semenza, Chemotherapy triggers HIF-1-dependent glutathione synthesis and copper chelation that induces the breast cancer stem cell phenotype, Proc. Natl. Acad. Sci. U. S. A. 112 (2015) E4600-4609.

ACCEPTED MANUSCRIPT

ACCEPTED MANUSCRIPT

▪Glucose-installed nanoparticle (Glu-NP) was made for cancer stem cell-targeted siRNA delivery.
▪Glu-NP was made by conjugating unimer polyion complexes on Au nanoparticle.
▪Enhanced cellular uptake of Glu-NP was observed in cancer stem cells in spheroid culture.
▪Glu-NP loaded with PLK1 siRNA suppressed growth of orthotopic breast tumor model.

ACCEPTED MANUSCRIPT